Biochimica et Biophysica Acta 1788 (2009) 1358–1365

Contents lists available at ScienceDirect

Biochimica et Biophysica Acta

journal homepage: www.elsevier.com/locate/bbamem

Cytochrome *c* induces lipid demixing in weakly charged phosphatidylcholine/phosphatidylglycerol model membranes as evidenced by resonance energy transfer

Galyna P. Gorbenko [a,*], Valeriya M. Trusova [a], Julian G. Molotkovsky [b], Paavo K.J. Kinnunen [c]

[a] Department of Biological and Medical Physics, V.N. Karazin Kharkiv National University, 4 Svobody Sq., Kharkiv, 61077, Ukraine
[b] Shemyakin-Ovchinnikov Institute of Bioorganic Chemistry, Russian Academy of Sciences, 16/10 Miklukho-Maklaya, Moscow, 117871, Russia
[c] Helsinki Biophysics and Biomembrane Group, Institute of Biomedicine, P.O. Box 63, Haartmaninkatu 8, University of Helsinki, FIN-00014, Finland

ARTICLE INFO

Article history:
Received 19 December 2008
Received in revised form 11 March 2009
Accepted 16 March 2009
Available online 25 March 2009

Keywords:
Resonance energy transfer
Cytochrome *c*
Protein–lipid interactions
Heme bilayer location
Lipid demixing

ABSTRACT

Resonance energy transfer (RET) between anthrylvinyl-labeled phosphatidylcholine (AV-PC) or phosphatidylglycerol (AV-PG) as donors and the heme groups of cytochrome *c* (cyt *c*) as acceptors was examined in PC/PG model membranes containing 10, 20 or 40 mol% PG with an emphasis on evaluating lipid demixing caused by this protein. The differences between AV-PC and AV-PG RET profiles observed at PG content 10 mol % were attributed to cyt *c* ability to produce segregation of acidic lipids into lateral domains. The radius of lipid domains recovered using Monte-Carlo simulation approach was found not to exceed 4 nm pointing to the local character of cyt *c*-induced lipid demixing. Increase of the membrane PG content to 20 or 40 mol% resulted in domain dissipation as evidenced by the absence of any RET enhancement while recruiting AV-PG instead of AV-PC.

1. Introduction

Among a variety of functionally relevant features of biological membranes one of the most essential is associated with their structural heterogeneity. High lateral mobility and chemical diversity of lipids and proteins favor the formation of nanometer to micrometer length scale regions differing from a bulk by their composition and physicochemical properties — membrane domains. These structures currently attract increasingly growing interest stimulated by their significant role in a number of cellular events including exocytosis, regulating the enzyme activity, modulating protein–membrane binding, signalling etc. [1]. A novel approach in molecular medicine, called membrane–lipid therapy considers membrane domains as a new target in the treatment of several human disorders [2].

To detect inhomogeneities in the lateral organization of cellular and model membranes, a range of powerful physical techniques have been employed, including atomic force microscopy [3], small-angle neutron scattering [4], fluorescence microscopy [5], fluorescence correlation spectroscopy [6], electron paramagnetic resonance [7], Fourier transform infrared spectroscopy [8], and resonance energy transfer [9]. Despite the great progress made in the past decade, the factors initiating and regulating domain formation still remain largely unknown. Characterization of nanoscale domains is particularly challenging, because of their highly dynamic nature and the size lying beyond the resolution of light microscopy. In this regard, fluorescence techniques, mainly resonance energy transfer (RET) seems to be especially promising. RET efficiency sensitively depends on the separation of donor and acceptor fluorophores on a scale 1–10 nm, their lateral distribution in a membrane and acceptor surface density. This makes RET technique potentially suitable for deducing the size of nanoscale domains, the fraction of membrane area occupied by these structures, the density of fluorophores confined within domains, and the mechanism of lateral reorganization of membrane constituents.

One type of membrane heterogeneity is represented by the domains formed upon adsorption of cationic proteins or peptides to negatively charged mixed bilayers. Lateral redistribution of anionic and neutral lipids has been induced, particularly, by cytochrome *c* [10,11], cardiotoxin II [12], polylysine [13] and basic peptides [14,15]. Existing theoretical models for this phenomenon emphasize the importance of both electrostatic and nonelectrostatic (elastic membrane deformation) forces and consider two possibilities: (i) formation of macroscopic protein–lipid domains enriched in acidic lipids, and (ii) local lipid demixing implicating molecular scale deviation from the average lipid composition within and around protein–membrane interaction zone [15–18]. Our previous studies on resonance energy transfer between tryptophan residues as donors and anthrylvinyl-labeled phosphatidylcholine (AV-PC) or phosphatidylglycerol (AV-PG) as acceptors revealed local demixing of PC and PG upon adsorption of lysozyme onto PC/PG lipid bilayers [19]. In the present study we employed RET technique to define demixing-favoring conditions and the extent of lipid redistribution produced

* Corresponding author. 52-52 Tobolskaya Str., Kharkiv, 61072, Ukraine.
E-mail address: galyna.p.gorbenko@univer.kharkov.ua (G.P. Gorbenko).

0005-2736/$ – see front matter © 2009 Elsevier B.V. All rights reserved.
doi:10.1016/j.bbamem.2009.03.007

by cytochrome *c*, another basic protein functioning as a component of mitochondrial respiratory chain. Although preferential association of cyt *c* with anionic lipids has long been established with a wide range of spectroscopic approaches [20–23], this property has been insufficiently scrutinized within the context of domain formation. Further in-depth evaluation of domain-forming potential of cyt *c* seems to be of importance in at least two regards. First, modulation of cyt *c* affinity for the inner mitochondrial membrane by lateral reorganization of the constituting lipids may prove essential not only for electron-transfer function of this protein, but also for its propensity to trigger programmed cell death, which presumably involves dissociation of cyt *c*–cardiolipin complexes [24]. Second, systematic studies of domain assembly in a wide variety of protein–lipid systems represent an effective way for identifying structural and physicochemical determinants of protein-induced lipid segregation.

2. Materials and methods

2.1. Chemicals

Bovine heart cyt *c* (oxidized form) and HEPES were purchased from Sigma (St. Louis, MO, USA). 1-palmitoyl-2-oleoyl-*sn*-glycero-3-phosphocholine (POPC) and 1-palmitoyl-2-oleoyl-*sn*-glycero-3-phospho-*rac*-glycerol (POPG) were from Avanti Polar Lipids (Alabaster, AL). Fluorescent lipids, 1-acyl-2-[12-(9-anthryl)-11-*trans*-dodecenoyl]-*sn*-glycero-3-phosphocholine (AV-PC), and 1-acyl-2-[12-(9-anthryl)-11-*trans*-dodecenoyl]-*sn*-glycero-3-phospho-1-*rac*-glycerol (AV-PG) were synthesized as described in detail elsewhere [25,26]. All other chemicals were of analytical grade.

2.2. Preparation of lipid vesicles

Large unilamellar vesicles were prepared by extrusion from PC mixtures with PG (10, 20 or 40 mol%). A thin lipid film was first formed from the lipid solutions in chloroform by removing the solvent under a stream of nitrogen. The dry lipid residues were subsequently hydrated with 20 mM HEPES, 0.1 mM EDTA, pH 7.4 at room temperature with lipid concentration of 1 mM. Thereafter, the sample was subjected to 15 passes through a 100-nm pore size polycarbonate filter (Millipore, Bedford, USA), yielding liposomes of desired composition. AV-PC or AV-PG (0.9 mol% of total lipid) was added to the mixture of PC and PG prior to the solvent evaporation. The concentration of fluorescent lipid was determined spectrophotometrically using anthrylvinyl extinction coefficient $E_{367}=9\times10^3\mathrm{M}^{-1}\mathrm{cm}^{-1}$ [25]. Hereafter, liposomes containing 10, 20 or 40 mol% POPG are referred to as PG10, PG20 or PG40, with the subscript denoting the type of energy donor (AV-PC or AV-PG).

2.3. Fluorescence measurements

Fluorescence measurements were performed at 25 °C using 10-mm path-length quartz cuvettes using spectrofluorimeter equipped with a magnetically stirred, thermostated cuvette holder (LS-50B, Perkin-Elmer Ltd., Beaconsfield, UK). AV-PC or AV-PG emission spectra were recorded with 367 nm excitation wavelength. Excitation and emission slit widths were set at 5 nm. Fluorescence intensity measured in the presence of cyt *c* at the maximum of AV emission (434 nm) was corrected for reabsorption and inner filter effects using the following coefficients [27]:

$$k=\frac{\left(1-10^{-A_o^{ex}}\right)\left(A_o^{ex}+A_a^{ex}\right)}{\left(1-10^{-\left(A_o^{ex}+A_a^{ex}\right)}\right)A_o^{ex}}\frac{\left(1-10^{-A_o^{em}}\right)\left(A_o^{em}+A_a^{em}\right)}{\left(1-10^{-\left(A_o^{em}+A_a^{em}\right)}\right)A_o^{em}} \quad (1)$$

where A_o^{ex}, A_o^{em} are the donor optical densities at the excitation and emission wavelengths in the absence of acceptor, A_a^{ex}, A_a^{em} are the acceptor optical densities at the excitation and emission wavelengths, respectively. The efficiency of energy transfer was determined by measuring the decrease of AV fluorescence upon addition of cyt *c*:

$$E=1-\frac{Q_{DA}}{Q_D}=1-Q_r \quad (2)$$

where Q_D, Q_{DA} are the donor quantum yields in the absence and presence of acceptors, respectively, Q_r is the relative quantum yield.

Steady-state fluorescence anisotropy of AV fluorophore was measured at excitation and emission wavelengths of 367 and 434 nm, respectively, with excitation and emission band passes set at 10 nm.

3. Theoretical background

3.1. Adsorption model

Cyt *c* binding to model membranes has been analyzed in terms of the adsorption model based on scaled particle (SPT) and Gouy–Chapman double-layer theories. This model allows for excluded area interactions between the adsorbing protein molecules and dependence of binding energy on the membrane surface coverage.

In the case of non-associating ligand and monomodal adsorption the scaled particle theory isotherm is described by the expressions [28]:

$$K_aF=\Phi\gamma(\Phi) \quad (3)$$

$$ln\gamma=-ln(1-\Phi)-\varepsilon-1+\frac{1}{1-\Phi}+\frac{\varepsilon}{(1-\Phi)^2} \quad (4)$$

where K_a is the association constant, F is the concentration of the protein free in solution, γ is the activity coefficient of adsorbed ligand, Φ is the fraction of surface area occupied by the adsorbed protein, $\Phi=nB/L_{out}$, B is the concentration of bound protein, n is the number of lipid molecules covered by a single protein, L_{out} is the concentration of accessible lipids related to total lipid concentration (L) as $L_{out}=0.5L$, and ε is a shape parameter (for disc-like ligand $\varepsilon=1$).

The equilibrium binding constant is treated as consisting of electrostatic (K_{el}) and intrinsic or nonelectrostatic (K_o) terms: $K_a=K_{el}K_o$. Electrostatic component of binding constant, dependent on electrostatic surface potential, environmental conditions (pH, ionic strength), and degree of surface coverage by a protein is given by [29]:

$$K_{el}=exp\left(-\frac{d}{dN_P}\left[\frac{\Delta F_{el}(N_P)}{k_BT}\right]\right) \quad (5)$$

where T is the temperature, k_B is Boltzmann's constant, and ΔF_{el} is the total gain in electrostatic free energy, being a function of the number of adsorbed protein molecules, $N_P=BN_A$:

$$\Delta F_{el}(N_P)=F_{el}^s(N_P)-F_{el}^s(0)-N_PF_{el}^P \quad (6)$$

where F_{el}^s and F_{el}^p are the electrostatic free energies of a membrane surface and a protein, respectively. The electrostatic free energy of a spherical protein molecule with effective charge $+ze$ and uniform charge distribution can be written as [30]:

$$F_{el}^P=\frac{z^2e^2}{2\varepsilon R_P\left(1+R_P\sqrt{\frac{8\pi e^2N_Ac}{\varepsilon k_BT}}\right)} \quad (7)$$

with R_p standing for the protein radius, e the elementary charge, N_A Avogadro's number, ε the dielectric constant, and c the molar concentration of monovalent ions. In terms of the Gouy–Chapman

double-layer theory the electrostatic free energy of a membrane of area $S_m = S_L L_{out}$ is given by [31]:

$$F_{el}^{s} = \frac{2k_B T S_m}{e}\left(\sigma \sinh^{-1}\left(\frac{\sigma}{a}\right) - \sqrt{a^2+\sigma^2} + a\right); \quad a = \sqrt{2\pi^{-1}\varepsilon c N_A k_B T} \tag{8}$$

where S_L is the mean area per lipid molecule taken here as 0.65 nm^2 for PC and PG, σ is the surface charge density given by:

$$\sigma = \frac{-e}{S_m}\left(\frac{K_1 f_A L_{out}}{K_1 + [H^+]_b \exp\left(\frac{-e\psi_o}{k_B T}\right)} - zB\right) \tag{9}$$

here f_A is the mole fraction of anionic lipid, K_1 is ionization constant (for PG $K_1 = 3$), $[H^+]_b$ is the bulk proton concentration, ψ_o is electrostatic surface potential of a membrane related to the surface charge density as:

$$\psi_o = \frac{2k_B T}{e}\sinh^{-1}\left(\frac{\sigma}{a}\right). \tag{10}$$

Numerical solution of the set of Eqs. (3)–(10) yields theoretical isotherms that were fitted to the experimental data.

3.2. Analytical model of resonance energy transfer

The RET data obtained with PG20 and PG40 liposomes were quantitatively interpreted in terms of the model of energy transfer on a surface formulated by Fung and Stryer [32] and extended in our previous works [19,33] to allow for distance dependence of orientation factor in two-dimensional systems. Cytochrome *c*–lipid systems under study were treated as containing one acceptor plane located at a distance d_c from the membrane center and two donor planes separated by a distance d_t (Fig. 1). Given that separation of acceptor plane from the outer donor plane is $d_a = |d_c - d_1|$, while for the inner plane $d_a = d_c + d_2$, relative quantum yield of the donor is given by

$$Q_r = 0.5 \times \left(\int_0^\infty \exp(-\lambda)\exp\left[-C_a^s S_1(\lambda)\right]d\lambda + \int_0^\infty \exp(-\lambda)\exp\left[-C_a^s S_2(\lambda)\right]d\lambda\right) \tag{11}$$

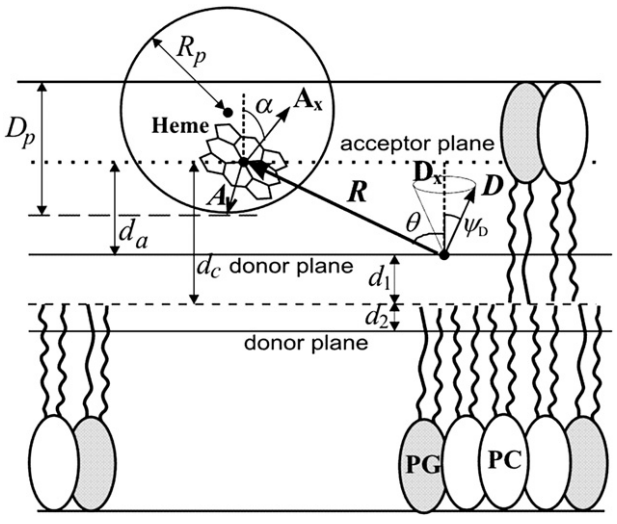

Fig. 1. Schematic representation of relative bilayer positions and angular relationships of donors (anthrylvinyl moiety of phosphatidylcholine or phosphatidylglycerol fluorescent derivatives) and acceptors (heme groups of cytochrome *c*) in a lipid bilayer.

$$S_1(\lambda) = \int_{|d_c - d_1|}^{\infty}\left[1 - \exp\left(-\lambda\kappa_1^2(R)\left(\frac{R_o^r}{R}\right)^6\right)\right]2\pi R dR \tag{12}$$

$$S_2(\lambda) = \int_{d_c + d_2}^{\infty}\left[1 - \exp\left(-\lambda\kappa_2^2(R)\left(\frac{R_o^r}{R}\right)^6\right)\right]2\pi R dR \tag{13}$$

where R is the donor–acceptor separation, $\lambda = t/\tau_d$; τ_d is the lifetime of excited donor in the absence of acceptor, C_a^s is the concentration of acceptors per unit area related to the molar concentrations of lipids accessible to protein binding and bound acceptor ($B_a = B$) as $C_a^s = B_a / L_{out} S_L$. By representing Förster radius as $R_o = [\kappa^2(R)]^{1/6} \cdot R_o^r$, it follows that

$$R_o^r = 979\left(n_r^{-4} Q_D J\right)^{1/6} \quad J = \frac{\int_0^\infty F_D(\lambda)\varepsilon_A(\lambda)\lambda^4 d\lambda}{\int_0^\infty F_D(\lambda)d\lambda} \tag{14}$$

here n_r is the refractive index of the medium ($n_r = 1.37$), Q_D is the donor quantum yield (0.8), J is the overlap between the donor emission ($F_D(\lambda)$) and acceptor absorption ($\varepsilon_A(\lambda)$) spectra [34]. When the donor emission and acceptor absorption transition moments are symmetrically distributed within the cones about certain axes D_x and A_x, distance-dependent orientation factor is given by [35]:

$$\kappa_{1,2}^2(R) = d_D d_A\left(3\left(\frac{d_c \mp 0.5 d_t}{R}\right)^2 - 1\right) + \frac{1 - d_D}{3} + \frac{1 - d_A}{3} + \left(\frac{d_c \mp 0.5 d_t}{R}\right)^2 (d_D - 2 d_D d_A + d_A) \tag{15}$$

$$d_{D,A} = \langle d_{D,A}^x \rangle\left(\frac{3}{2}\cos^2\alpha_{D,A} - \frac{1}{2}\right) \quad \langle d_{D,A}^x \rangle = \left(\frac{3}{2}\cos^2\psi_{D,A} - \frac{1}{2}\right) \tag{16}$$

where $\psi_{D,A}$ are the cone half-angles, $\alpha_{D,A}$ are the angles made by D_x and A_x with the bilayer normal ***N***. The axial depolarization factors $\langle d_D^x \rangle$ and $\langle d_A^x \rangle$ are related to the experimentally measurable steady-state (r) and fundamental (r_0) anisotropies of donor and acceptor [35]:

$$d_{D,A}^x = \pm\left(r_{D,A} / r_{0D,A}\right)^{1/2}. \tag{17}$$

3.3. Monte-Carlo calculations

The results of RET measurements in PG10$_{AV\text{-}PC}$ and PG10$_{AV\text{-}PG}$ liposomes suggesting lateral redistribution of PG and PC molecules upon cyt *c* binding were treated using a Monte-Carlo approach. Positions of donors and acceptors were generated randomly in a square cell assuming periodic boundary conditions to avoid edge effects. The relative quantum yield averaged over all donors was calculated from fluorophore coordinates as:

$$Q_r = \frac{1}{N_D}\sum_{j=1}^{N_D}\left[1 + \sum_{i=1}^{N_{AC}}\left(\frac{R_o^r \kappa^2\left(r_{ij}\right)}{r_{ij}}\right)^6\right]^{-1} \tag{18}$$

where N_D, N_{AC} stand for the number of donors and acceptors, respectively. The simulation procedure was repeated for at least 1000 fluorophore configurations until the standard deviation in Q_r was <2%. To test the simulation algorithm, we compared the RET data obtained using the above model of Fung and Stryer [32] and the Monte-Carlo calculation scheme. As illustrated in Fig. 2, the results from analytical and numerical simulation approaches are in good agreement.

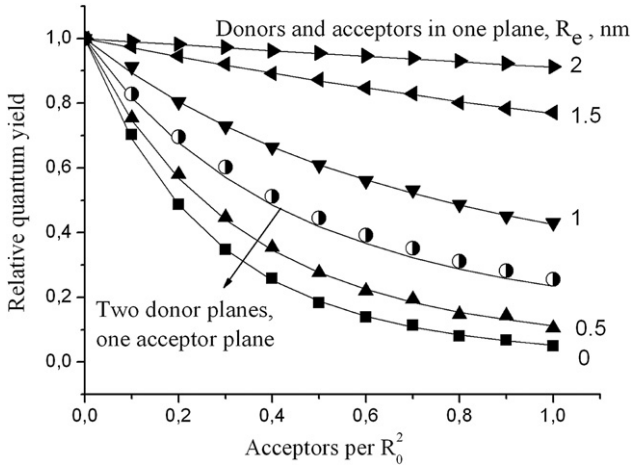

Fig. 2. Comparison of relative quantum yields of a donor calculated from the analytical model of Fung and Stryer (symbols) with those derived from the Monte-Carlo simulation (solid lines). R_e is the distance of closest approach between donor and acceptor. In the case of two donor planes and one acceptor plane the calculations were performed with $R_e = 0$, distance between acceptor plane and bilayer midplane $d_c = 3$ nm and separation of donor planes $d_t = d_1 + d_2 = 0.3$ nm.

While analyzing the case of protein-induced domain formation we assumed that total number of disk-shaped domains (N_{dm}) is equal to the number of membrane-bound protein molecules (B_a), i.e. $N_{dm} = B_a N_A$, N_A is Avogadro's number. Total number of lipid molecules and the number of PG (N_{PG}^{dm}) and PC (N_{PC}^{dm}) molecules in domains can be written as:

$$N_L^{dm} = N_{PG}^{dm} + N_{PC}^{dm} = \frac{B_a N_A \pi r_{dm}^2}{S_L}; \quad N_{PG}^{dm} = f_{PG} k N_L^{dm};$$
$$N_{PC}^{dm} = (1 - f_{PG}k) N_L^{dm} \tag{19}$$

where k is the ratio of PG concentrations in the protein-affected region (adsorption domain of radius r_{dm}) at nonrandom and random distribution of charged lipids. For molar fraction of donors (AV-PC or AV-PG) f_D, total number of AV-PC or AV-PG molecules in outer monolayer is given by:

$$N_{AV-PC}^{tot} = N_{AV-PG}^{tot} = L_{out} f_D N_A. \tag{20}$$

Given that the fraction of PG (f_{PG}^{dm}) and PC (f_{PC}^{dm}) in domains is equal to

$$f_{PG}^{dm} = \frac{B_a N_A f_{PG} k \pi r_{dm}^2}{L_{out} N_A f_{PG} S_L} = \frac{B_a k \pi r_{dm}^2}{L_{out} S_L}; \quad f_{PC}^{dm} = \frac{B_a \pi r_{dm}^2 (1 - f_{PG}k)}{L_{out} S_L (1 - f_{PG})} \tag{21}$$

the number of AV-PG molecules in domain ($N_{AV\text{-}PG}^{dm}$) and non-domain ($N_{AV\text{-}PG}^{ndm}$) regions can be expressed as:

$$N_{AV-PG}^{dm} = N_{AV-PG}^{tot} f_{PG}^{dm} = \frac{B_a k \pi r_{dm}^2 N_A f_D}{S_L};$$
$$N_{AV-PG}^{ndm} = L_{out} N_A f_D - N_{AV-PG}^{dm}. \tag{22}$$

Surface densities of AV-PG in domain ($\delta_{AV\text{-}PG}^{dm}$) and non-domain ($\delta_{AV\text{-}PG}^{ndm}$) regions are given by:

$$\delta_{AV-PG}^{dm} = \frac{N_{AV-PG}^{dm}}{B_a N_A \pi r_{dm}^2} = \frac{f_D k}{S_L};$$
$$\delta_{AV-PG}^{ndm} = \frac{N_{AV-PG}^{ndm}}{L_{out} S_L N_A - B_a N_A \pi r_{dm}^2} = \frac{f_D \left(L_{out} S_L - k B_a \pi r_{dm}^2 \right)}{S_L \left(L_{out} S_L - B_a \pi r_{dm}^2 \right)}. \tag{23}$$

Analogously, for AV-PC one obtains:

$$N_{AV-PC}^{dm} = N_{AV-PC}^{tot} f_{PC}^{dm} = \frac{B_a \pi r_{dm}^2 N_A f_D (1 - f_{PG}k)}{S_L (1 - f_{PG})};$$
$$N_{AV-PC}^{ndm} = L_{out} N_A f_D - N_{AV-PC}^{dm} \tag{24}$$

$$\delta_{AV-PC}^{dm} = \frac{N_{AV-PC}^{dm}}{B_a N_A \pi r_{dm}^2} = \frac{f_D (1 - f_{PG}k)}{S_L (1 - f_{PG})};$$
$$\delta_{AV-PC}^{ndm} = \frac{f_D}{S_L (1 - f_{PG})} \left(1 - \frac{f_{PG} \left(L_{out} S_L - k B_a \pi r_{dm}^2 \right)}{L_{out} S_L - B_a \pi r_{dm}^2} \right). \tag{25}$$

Eqs. (23) and (25) were used to calculate the number of donors in domain and non-domain regions for a square cell with the side length taken as 10 R_o (here $R_o = 0.67$ R_o^r). The number of acceptors was determined by multiplying protein surface density (C_a^s) by the cell square (S_c) ($N_{AC} = C_a^s S_c$). The simulation program was scripted in Mathcad 2001 Professional.

4. Results

Resonance energy transfer between AV-PC or AV-PG and the heme group of cyt *c* was examined by monitoring the decrease of donor fluorescence upon addition of the acceptor. In Figs. 3 and 4 relative

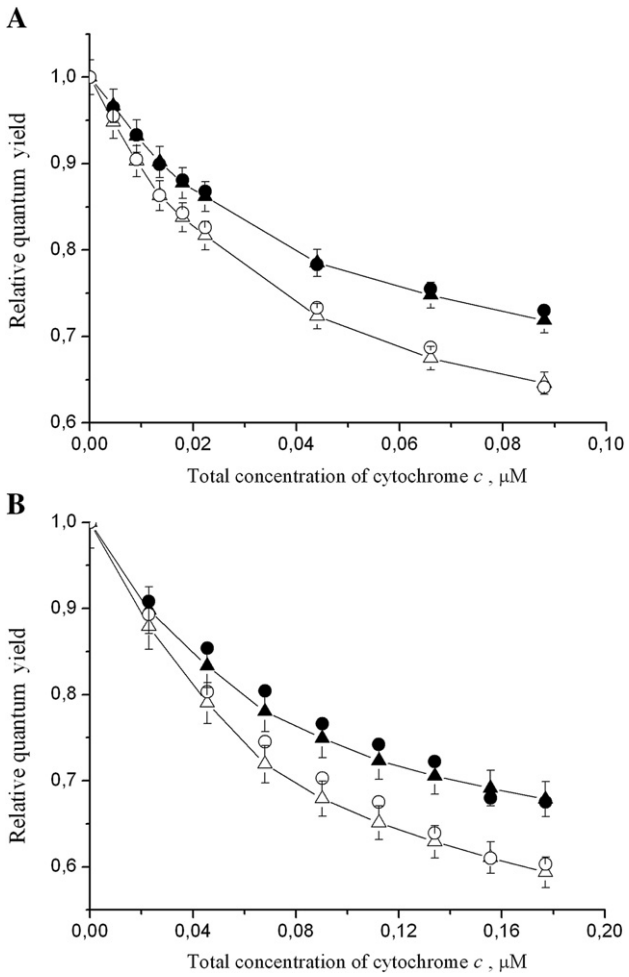

Fig. 3. Relative quantum yield of AV-PC and AV-PG in PC/PG liposomes containing 10 mol% PG as a function of cytochrome *c* concentration. Total lipid concentration (L): 5 μM (A), 20 μM (B). Experimental data are depicted by triangles: AV-PC (▲), AV-PG (△). The results from Monte-Carlo calculations ($d_c = 3.6$ nm, $n = 11, = 22$ μM^{-1}) are denoted by circles: AV-PC (●), AV-PG (○).

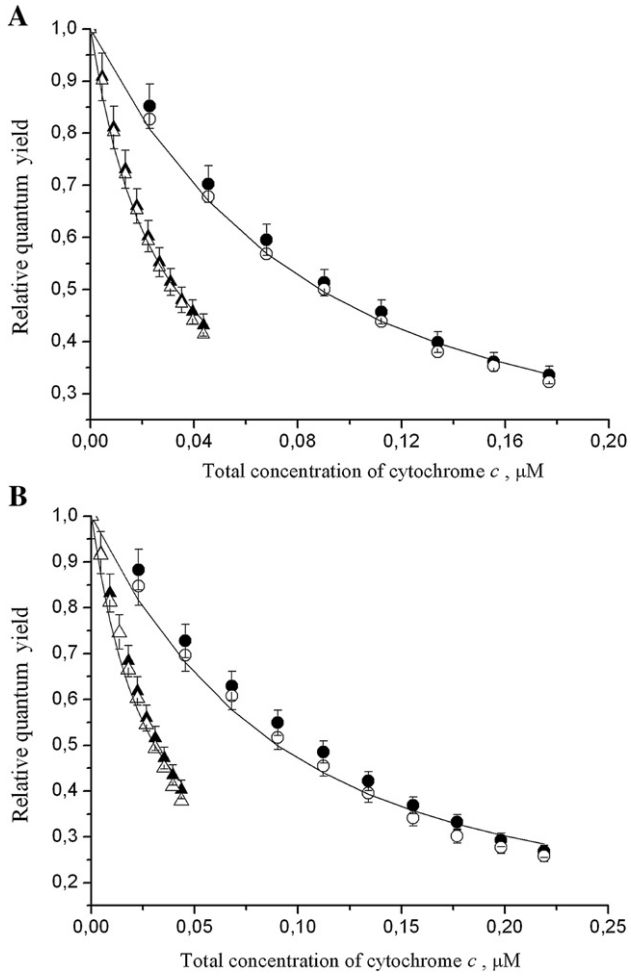

Fig. 4. Relative quantum yield of AV-PC and AV-PG in PC/PG liposomes containing 20 mol% PG (A) or 40 mol% PG (A) as a function of cytochrome *c* concentration. Experimental data are depicted by triangles and circles: AV-PC, $L=5$ μM (▲); AV-PG, $L=5$ μM (△); AV-PC, $L=20$ μM (●); AV-PG, $L=20$ μM (○). Solid lines show theoretical curves calculated from the analytical RET model (Eqs. (11)–(16)) with the following parameters: $d_c=2.1$ nm, $n=11$, $K_o=22$ μM^{-1}, $z=4.1$.

quantum yields of AV-PC and AV-PG are plotted as a function of cyt *c* concentration for different types of liposomes. It appeared that at the lowest PG content, 10 mol%, energy transfer from the anionic donor AV-PG is more efficient than that from neutral donor AV-PC. This can be interpreted as arising from an accumulation of acidic lipids in the vicinity of adsorbed protein. In contrast, the RET profiles observed for PG20 and PG40 liposomes are featured by the absence of any statistically significant difference between (i) relative quantum yields of AV-PC and AV-PG on the one hand and (ii) PG20 and PG40 Q_r values, on the other hand. The former observation suggests that cyt *c* is incapable of producing marked segregation of anionic lipids in the model membranes containing 20 or 40 mol% PG. This allowed us to quantitatively analyze PG20 and PG40 RET data in terms of the above analytical model (Eqs. (11)–(16)) describing energy transfer between donors and acceptors randomly distributed in two dimensions. Since such analysis requires knowing of surface acceptor concentration, 2D RET model was combined with the model of electrostatically controlled adsorption, in accordance with the approach developed in our previous works [36,37]. This approach permits simultaneous determination of both structural (heme distance from the bilayer center) and binding (intrinsic association constant) characteristics from the global fitting of multiple arrays of RET data acquired over a range of experimental conditions. The principal advantage of global analysis is associated with the possibility of the most correct estimation of the model parameters due to minimization of their cross-correlation [38]. In the present study optimization procedure was applied to the datasets obtained for two types of donors at varying PG mole fraction (0.2 or 0.4), protein and lipid concentrations. While choosing the model parameters tentatively divided into two categories, assigned and optimized, we proceed from the following considerations.

4.1. Assigned parameters

d_1, separation between the outer donor plane and bilayer midplane, was allowed to vary within the maximum possible limits 0–2.3 nm (membrane half-width) assuming that cytochrome *c* is capable of perturbing the donor position in the outer monolayer.

d_2, separation between the outer donor plane and bilayer midplane, was varied in the limits 0.15–0.3 nm, consistent with i) the size of AV fluorophore (ca. 0.7×0.3 nm), and ii) ^{1}H-NMR and fluorescence quenching data suggesting that in a lipid bilayer nonpolar AV moiety resides in the region of terminal methyl groups, preferentially orienting parallel to acyl chains [26,39].

d_D^x, donor depolarization factor, was calculated from Eq. (17), with fundamental anisotropy of anthrylvinyl fluorophore (r_{0D}) taken as 0.08 [40], and r_D value experimentally measured at excitation and emission wavelengths 367 and 430 nm, respectively (Fig. 5).

d_A^x, acceptor depolarization factor, was determined from Eq. (16), allowing for the linear dichroism data indicating that transition moment of cyt *c* lies within the porphyrin plane [41], i.e. $\psi_A=\pi/2$, $d_A^x=-0.5$.

α, the angle between porphyrin plane and bilayer surface, was taken on two limiting assumptions: $\alpha_A=0$ (porphyrin plane is parallel to bilayer surface) or $\alpha_A=\pi/2$ (porphyrin plane is perpendicular to bilayer surface), because preferable orientation of membrane-bound cyt *c* is not yet unequivocally defined.

n, the number of lipid molecules per molecule of bound protein was evaluated from geometric considerations. Cross-section of unperturbed cyt *c* molecule (8–9 nm^2) corresponds to the surface area occupied by 11–13 lipid headgroups. Taking into account that in the interfacial environment with lowered pH cyt *c* may undergo transition to a molten globule-like state [42] in which hydrodynamic radius of a protein was reported to increase by no more than 20% [43], parameter *n* was allowed to vary in the limits 11–19.

z, effective protein charge, was taken as 4.1, the value derived in our previous study from global analysis of the results of RET experiments conducted at varying pH, ionic strength, anionic lipid content, and protein-to-lipid molar ratio [36]. The fact that effective charge is less than net charge of cyt *c* (+9), is likely to arise from the limitations of

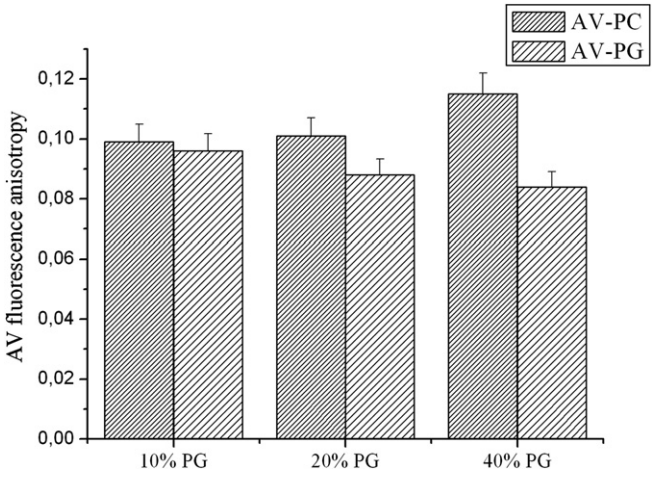

Fig. 5. Anthrylvinyl fluorescence anisotropy measured with $\lambda_{ex}=367$ nm and $\lambda_{em}=434$ nm for different types of PC/PG liposomes. Lipid concentration was 50 μM.

Table 1
Structural and binding parameters characterizing cyt *c* interaction with PC/PG model membranes containing 20 or 40 mol% PG.

Binding stoichiometry, *n*	Intrinsic association constant, K_o, μM^{-1}	Heme distance from bilayer center, d_c, nm		χ^2
		$\alpha_A=\pi/2$	$\alpha_A=0$	
11	22±4	2.3±0.4	2.0±0.6	9.1×10^{-4}
19	34±8	2.2±0.5	2.1±0.5	9.9×10^{-4}

double-layer theory, associated, particularly, with finite size of the protein relative to Debye length [29].

4.2. Optimized parameters

d_c, the distance between heme groups of cyt *c* (acceptor plane) and membrane midplane (Fig. 1). Maximum meaningful value of this parameter, corresponding to surface location of cyt *c*, can be estimated as $d_c^{max}=0.5\,d_m+R_p+r_t$, where d_m is the membrane width (4.6 nm), R_p is the protein radius (ca. 1.7 nm), while r_t stands for displacement of heme group off the molecule center (ca. 1.1 nm), thus yielding $d_c^{max}=5.1$ nm.

K_o, intrinsic association constant independent of the membrane surface charge. K_o represents invariant part of the association constant, while K_{el} is a function of acidic lipid mole fraction, degree of its protonation, ionic strength and surface coverage.

Allowing for predominant role of electrostatic forces in cyt *c* membrane interaction quantitative interpretation of the results presented here was based on the assumption that protein association with differently charged lipid bilayers can be consistently described in terms of the unified intrinsic association constant and binding stoichiometry. The values of K_o and d_c were estimated by nonlinear least-squares technique involving minimization of the following error function:

$$\chi^2=\frac{1}{N}\sum_{i=1}^{N}\left(Q_{ri}^{e}-Q_{ri}^{t}\right)^2 \tag{26}$$

where N is the total number of experimental points being simultaneously analyzed ($N=76$), Q_r^e is the experimental Q_r value, Q_r^t is the relative quantum yield calculated by numerical integration of Eqs. (11)–(17), with B_a being calculated numerically from the Eqs. (3)–(10).

The values of intrinsic association constant recovered from the global fit of PG20 and PG40 datasets (Table 1) were used to estimate the concentration of bound protein (B_a) for PG10 liposomes and then calculate the number of acceptors (N_{AC}) and donors ($N_{AV\text{-}PC,AV\text{-}PG}^{dm,ndm}$) in a simulation cell. This created a basis for implementation of the Monte-Carlo algorithm. For $PG10_{AV\text{-}PC}$ system, the number of donors in domains $N_{AV\text{-}PC}^{dm}$ proved to take on nonzero value ($N_{AV\text{-}PC}^{dm}=1$) only at the highest surface densities of cyt *c*, thereby rendering RET profiles insensitive to variations in domain radius (r_{dm}) and the extent of PG segregation in the interaction zone (k). Therefore, the RET data obtained for $PG10_{AV\text{-}PC}$ liposomes were treated using the Monte-Carlo approach with being the only optimized parameter. Next, the recovered value was fixed and (r_{dm},k) sets providing the best agreement between simulated and experimental data were derived from the Monte-Carlo analysis of $PG10_{AV\text{-}PG}$ RET curves.

5. Discussion

Cyt *c*–lipid interactions have long been in a focus of considerable research efforts yielding insights into a number of molecular level details of this process, viz. i) essentially electrostatic nature of cyt *c* complexation with lipids [20–22], ii) coverage-dependent protein insertion into membrane interior [23,44,45], and iii) destabilizing effect of anionic lipids on cyt *c* tertiary structure [42,46,47], and iv) structural reorganization of composite membranes upon protein binding [10,11]. The present RET study of cyt *c* association with negatively charged lipid bilayers provided quantitative information about protein location relative to lipid–water interface and the degree of lipid demixing in PC/PG model membranes depending on PG mole fraction. The observation that in PG20 and PG40 systems the efficiencies of energy transfer are similar for neutral (AV-PC) and negatively charged (AV-PG) donors has led us to assume that in these types of liposomes cyt *c* does not cause PG molecules to accumulate in the interaction zone, i.e. lipid distribution is close to random. This assumption, together with the idea that cyt *c* binding to PC/PG membranes differing in PG proportion is governed by identical, primarily electrostatic mechanisms, provide the prerequisites for PG20 and PG40 data to be globally analyzed in terms of the combined RET-adsorption model. The recovered values of intrinsic association constant ensuring the best agreement between the calculated and experimental relative quantum yields of AV-PC and AV-PG, were found to fall in the range 20–40 μM^{-1}. Multiplying these K_o values by electrostatic term K_{el}, which depends on PG proportion, ionic strength, pH and degree of membrane coverage with the protein (Eqs. (5)–(10)), yields effective binding constants K_a of the magnitude 10^5–10^6 M^{-1}. As illustrated in Fig. 6, K_a increases with PG mole fraction, but decreases with cyt *c* concentration due to screening of the membrane surface charge by the adsorbed protein.

Another parameter recovered from the global data analysis is d_c, the distance between the heme groups of cyt *c* and the bilayer midplane. In the model membranes containing 20 or 40 mol% PG this distance was found to lie between 1.6 and 2.7 nm.

Notably, the errors given in Table 1 for estimates were obtained assuming the possibility of protein-induced displacement of the donors located in the outer monolayer from the membrane core to interfacial region. Such a possibility, together with the uncertainty in heme position within interfacially loosened protein structure does not allow us to draw unambiguous conclusions on the depth of cytochrome *c* membrane penetration. It is noteworthy in this respect that the mode of cyt *c* membrane interaction has been found to depend on the surface coverage [23,44]. Peripheral electrostatic binding prevails at low protein surface densities (L_{out}/P ratios greater than 20) while at L_{out}/P ratios approaching the saturation coverage (ca. 11) cyt *c* tends to penetrate into membrane interior [23]. It has been hypothesized that protein insertion into lipid bilayer is triggered by a certain critical surface coverage at which lateral pressure of two-dimensional "adsorbate gas" is close to its threshold value [45]. Since the lowest L_{out}/P value reached in our experiments is 80 (43 on assumption of complete protein binding) it might be expected that cyt

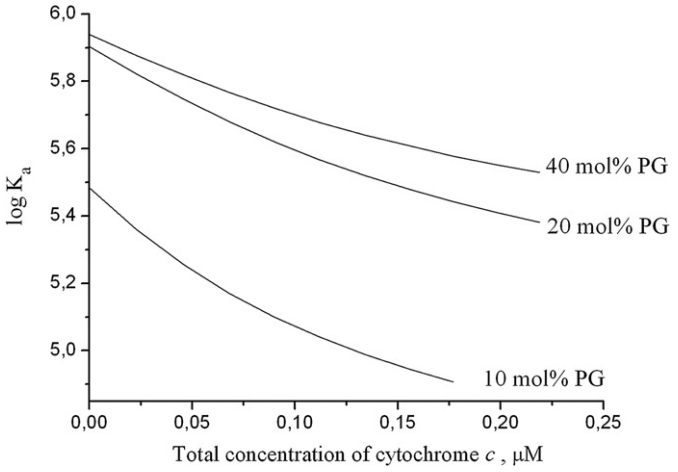

Fig. 6. Coverage-dependent association constants calculated from Eqs. (5)–(10) with $K_o=22$ μM^{-1}.

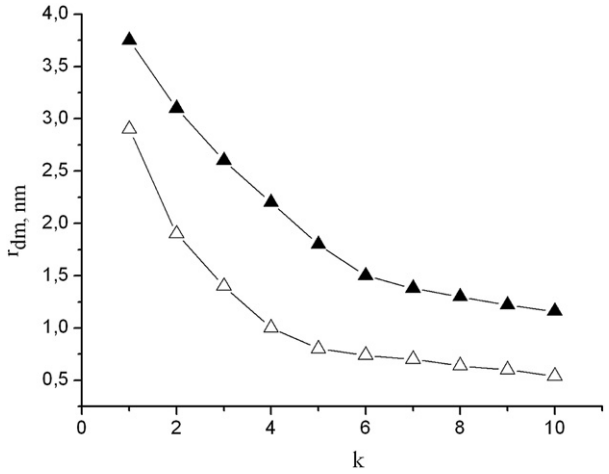

Fig. 7. Relationships between the radius of lipid domains (r_{dm}) and a factor by which PG mole fraction increases in the protein–membrane interaction zone (k) obtained by the Monte-Carlo simulations. Cyt c surface density was calculated from Eqs. (3)–(10) for $n=11$, $K_o=22$ μM^{-1} (▲); or $n=19$, $K_o=34$ μM^{-1} (△).

c association with the model membrane under study is mainly driven by electrostatic forces.

In contrast to PG20 and PG40 vesicles, where the RET curves obtained for either AV-PC or AV-PG as energy donors were virtually indistinguishable, PG10 energy transfer from AV-PG was more effective compared to AV-PC (Fig. 3). The observed differences between $PG10_{AV\text{-}PC}$ and $PG10_{AV\text{-}PG}$ RET profiles are most likely to originate from lateral redistribution of PG and PC molecules accompanied by enrichment of the interaction zone with acidic lipids. To account for this effect we designed the Monte-Carlo simulation in which AV-PG donors were considered as being randomly distributed within disk-shaped domains of radius r_{dm} centered at each acceptor's location. Our main goal was to determine characteristic domain size, i.e. dimensions of the protein-affected region where PG concentration is k times higher than that for a random lipid distribution. Simulation-based fitting of $PG10_{AV\text{-}PC}$ and $PG10_{AV\text{-}PG}$ RET data with k being varied from 1 to 10 (the value corresponding to complete replacement of PC with PG) has revealed that the size of the zone with increased PG concentration does not exceed 4 nm (Fig. 7). The fact that the recovered r_{dm} estimates are of the same order of magnitude as the protein diameter (ca. 3.4 nm) is strongly suggestive of cyt c property to induce local demixing of PG and PC molecules in PG10 membranes. Notably, d_c values recovered for PG10 systems (3.6 nm) were greater than those for PG20 and PG 40 systems suggesting shallower protein location at PG content 10 mol%.

Taken together, our results are in good agreement with the predictions of theoretical model proposed by May et al. [16]. This model considers domain formation triggered by the adsorption of basic globular proteins on the surface of binary lipid membranes with varying proportions of acidic lipids. Based on minimization of a mean-field free energy functional and further numerical solution of Poisson–Boltzmann equation, the authors evaluated the extent of lipid redistribution for the cases of (i) equal surface charged densities of the protein and the membrane; (ii) a weakly charged protein, highly charged membranes; and (iii) a highly charged protein, and a weakly charged membrane. The most pronounced exchange of the neutral and acidic lipids in the interaction zone was found to occur in the last case, when highly charged protein adsorbs on weakly charged membrane, with the extent of lipid segregation being determined by the balance between the gain in electrostatic adsorption energy and the loss of lipid mixing entropy. It is noteworthy in this context that not only electrostatic, but also nonelectrostatic mechanisms associated with membrane elasticity may lower the interaction free energy thereby favoring the domain formation [16–18].

In conclusion, the present study clearly demonstrates that the lipid-segregating propensity of cyt c can be controlled by the membrane surface charge density. As follows from the comparison of energy transfer efficiencies in PC/PG systems containing anthrylvinyl-labeled neutral (AV-PC) or negatively charged (AV-PG) donors, at PG content 10 mol%, cyt c produces formation of lateral domains enriched in acidic lipids, while at higher PG mole fractions (20 and 40 mol%) lipid distribution is close to random. The size of lipid domains deduced from the Monte-Carlo analysis of PG10 RET data proved to be comparable to cyt c dimensions suggesting that lipid demixing takes place locally, in the immediate vicinity of the adsorbed protein. The revealed peculiarities of cyt c lipid interactions may have important functional implications as a means of modulating electron-transfer and apoptotic propensities of this protein.

Acknowledgements

This work was supported by the grant No. 4534 from the Science and Technology Center in Ukraine. GG gratefully acknowledges a visiting scientist award by the Sigrid Juselius Foundation. HBBG is supported by the Finnish Academy and Sigrid Juselius Foundation.

References

[1] J.C.M. Holthuis, G. Vanmeer, K. Huitema, Lipid microdomains, lipid translocation and the organization of intracellular membrane transport, Mol. Membr. Biol. 20 (2003) 231–241.
[2] P.V. Escriba, J.M. Gonzales-Ros, F.M. Goni, P.K.J. Kinnunen, L. Vign, L. Sanchez-Magraner, A.M. Fernandez, X. Busquets, I. Horvath, G. Barcelo-Coblijn, Membranes: a meeting point for lipids, proteins and therapies, J. Cell. Mol. Med. 12 (2008) 829–875.
[3] L.K. Nielsen, A. Vishnyakov, K. Jorgensen, T. Bjornholm, O.G. Mouritsen, Nanometer-scale structure of fluid lipid membranes, J. Phys. Condens. Matter 12 (2000) A309–A314.
[4] J. Pencer, T. Mills, V. Anghel, S. Krueger, R. Epand, J. Katsaras, Detection of submicron-sized raft-like domains in membranes by small-angle neutron scattering, Eur. Phys. J. E. 18 (2005) 447–458.
[5] S. Veatch, S. Keller, Seeing spots: complex phase behavior in simple membranes, Biochim. Biophys. Acta 1746 (2005) 172–185.
[6] J. Korlach, T. Baumgart, W.W. Webb, G.W. Feigenson, Detection of motional heterogeneities in lipid bilayer membranes by dual probe fluorescence correlation spectroscopy, Biochim. Biophys. Acta 1668 (2005) 158–163.
[7] M.B. Sankaram, D. Marsh, T.E. Thompson, Determination of fluid and gel domain sizes in two-component, two-phase lipid bilayers: an electron spin resonance spin label study, Biophys. J. 63 (1992) 340–349.
[8] R. Mendelsohn, D.J. Moore, Vibrational spectroscopic studies of lipid domains in biomembranes and model systems, Chem. Phys. Lipids 96 (1998) 141–157.
[9] L.M.S. Loura, A. Fedorov, M. Prieto, Fluid–fluid membrane microheterogeneity: a fluorescence resonance energy transfer study, Biophys. J. 80 (2001) 776–788.
[10] D. Haverstick, M. Glaser, Influence of proteins on the reorganization of phospholipid bilayers into large domains, Biophys. J. 55 (1989) 677–682.
[11] T. Heimburg, B. Angerstein, D. Marsh, Binding of peripheral proteins to mixed lipid membranes: effect of lipid demixing upon binding, Biophys. J. 76 (1999) 2575–2586.
[12] M.A. Carbone, P.M. Macdonald, Cardiotoxin II segregates phosphatidylglycerol from mixtures with phosphatidylcholine: ^{31}P and ^{2}H NMR spectroscopic evidence, Biochemistry 35 (1996) 3368–3378.
[13] C.M. Franzin, P.M. Macdonald, Polylysine-induced ^{2}H NMR observable domains in phosphatidylserine/phosphatidylcholine lipid bilayers, Biophys. J. 81 (2001) 3346–3362.
[14] K. Gawrisch, J.A. Barry, L.L. Holte, T. Sinnwell, L.D. Bergelson, J.A. Ferretti, Role of interactions at the lipid–water interface for domain formation, Mol. Membr. Biol. 12 (1995) 83–88.
[15] G. Denisov, S. Wanaski, P. Luan, M. Glaser, S. McLaughlin, Binding of basic peptides to membranes produces lateral domains enriched in the acidic lipids phosphatidylserine and phosphatidylinositol-4,5-bisphosphate: an electrostatic model and experimental results, Biophys. J. 74 (1998) 731–744.
[16] S. May, D. Harries, A. Ben-Shaul, Lipid demixing and protein–protein interactions in the adsorption of charged proteins on mixed membranes, Biophys. J. 79 (2000) 1747–1760.
[17] E.C. Mbamala, A. Ben-Shaul, S. May, Domain formation induced by the adsorption of charged proteins on mixed lipid membranes, Biophys. J. 88 (2005) 1702–1714.
[18] M.M. Sperotto, O.G. Mouritsen, Lipid enrichment and selectivity of integral membrane proteins in two-component lipid bilayers, Eur. Biophys. J. 22 (1993) 323–328.
[19] G.P. Gorbenko, V.M. Ioffe, J.G. Molotkovsky, P.K.J. Kinnunen, Resonance energy transfer study of lysozyme–lipid interactions, Biochim. Biophys. Acta 1778 (2008) 1213–1221.

[20] T. Heimburg, P. Hildebrandt, D. Marsh, Cytochrome *c*–lipid interactions studied by resonance Raman and ^{31}P NMR spectroscopy. Correlation between the conformational changes of the protein and lipid bilayer, Biochemistry 30 (1991) 9084–9089.
[21] M. Rytömaa, P.K.J. Kinnunen, Evidence for two distinct acidic phospholipid-binding sites in cytochrome *c*, J. Biol. Chem. 269 (1994) 1770–1774.
[22] Z. Salamon, G. Tollin, Surface plasmon resonance studies of complex formation between cytochrome *c* and bovine cytochrome *c* oxidase incorporated into a supported planar lipid bilayer. I. Binding of cytochrome *c* to cardiolipin/phosphatidylcholine membranes in the absence of oxidase, Biophys. J. 71 (1996) 848–857.
[23] S. Oellerich, S. Lecomte, M. Paternostre, T. Heimburg, P. Hildebrandt, Peripheral and integral binding of cytochrome *c* to phospholipids vesicles, J. Phys. Chem. 108 (2004) 3871–3878.
[24] X.J. Jiang, X.D. Wang, Cytochrome *c*-mediated apoptosis, Annu. Rev. Biochem. 73 (2004) 87–106.
[25] L. Bergelson, J. Molotkovsky, Y. Manevich, Lipid-specific probes in studies of biological membranes, Chem. Phys. Lipids 37 (1985) 165–195.
[26] J. Molotkovsky, M. Smirnova, M. Karyukhina, L. Bergelson, Synthesis of anthrylvinyl phospholipids probes, Bioorg. Khim. (Moscow) (Engl. Transl.) 15 (1989) 377–380.
[27] A.A. Bulychev, V.N. Verchoturov, B.A. Gulaev, Current Methods of Biophysical Studies, Vyschaya shkola, Moscow, 1988.
[28] R. Chatelier, A.P. Minton, Adsorption of globular proteins on locally planar surfaces: models for the effect of excluded surface area and aggregation of adsorbed protein on adsorption equilibria, Biophys. J. 71 (1996) 2367–2374.
[29] T. Heimburg, D. Marsh, Protein surface-distribution and protein–protein interactions in the binding of peripheral proteins to charged lipid membranes, Biophys. J. 68 (1995) 536–546.
[30] C. Tanford, The electrostatic free energy of globular protein ions in aqueous solution, J. Phys. Chem. 59 (1955) 788–793.
[31] F. Jahnig, Electrostatic free energy and shift of the phase transition for charged lipid membranes, Biophys. Chem. 4 (1976) 309–318.
[32] B.K. Fung, L. Stryer, Surface density determination in membranes by fluorescence energy transfer, Biochemistry 17 (1978) 5241–5248.
[33] G. Gorbenko, T. Handa, H. Saito, J. Molotkovsky, M. Tanaka, M. Egashira, M. Nakano, Effect of cholesterol on bilayer location of the class A peptide Ac-18A-NH_2 as revealed by fluorescence resonance energy transfer, Eur. Biophys. J. 32 (2003) 703–709.
[34] J.R. Lakowicz, Principles of Fluorescent Spectroscopy, Plenum Press, New York, 1999.
[35] R. Dale, J. Eisinger, W. Blumberg, The orientational freedom of molecular probes. The orientation factor in intramolecular energy transfer, Biophys. J. 26 (1979) 161–194.
[36] G.P. Gorbenko, J.G. Molotkovsky, P.K.J. Kinnunen, Cytochrome *c* interaction with cardiolipin/phosphatidylcholine model membranes: effect of cardiolipin protonation, Biophys. J. 90 (2006) 4093–4103.
[37] Ye.A. Domanov, G.P. Gorbenko, J.G. Molotkovsky, Global analysis of steady-state energy transfer measurements in membranes: resolution of structural and binding parameters, J. Fluoresc. 14 (2004) 49–55.
[38] J.M. Beechem, Global analysis of biochemical and biophysical data, Meth. Enzymol. 210 (1992) 37–54.
[39] I. Boldyrev, X. Zhai, M.M. Momsen, H.L. Brockman, R.E. Brown, J.G. Molotkovsky, New BODIPY lipid probes for fluorescence studies of membranes, J. Lipid Res. 48 (2007) 1518–1532.
[40] L. Johansson, J. Molotkovsky, L. Bergelson, Fluorescence properties of anthrylvinyl lipid probes, Chem. Phys. Lipids 53 (1990) 185–189.
[41] W.A. Eaton, R.M. Hochstrasser, Electronic spectrum of single crystals of ferricytochrome *c*, J. Chem. Phys. 46 (1967) 2533–2538.
[42] T.J.T. Pinheiro, G.A. Elöve, A. Watts, H. Roder, Structural and kinetic description of cytochrome *c* unfolding induced by the interaction with lipid vesicles, Biochemistry 36 (1997) 13122–13132.
[43] O.B. Ptitsyn, D.A. Dolgich, R.I. Gilmanshin, Fluctuating state of protein globule, Mol. Biol. 17 (1983) 569–576.
[44] Y.A. Domanov, J.G. Molotkovsky, G.P. Gorbenko, Coverage-dependent changes of cytochrome *c* transverse location in phospholipid membranes revealed by FRET, Biochim. Biophys. Acta 1716 (2005) 49–58.
[45] M.J. Zuckermann, T. Heimburg, Insertion and pore formation driven by adsorption of proteins onto lipid bilayer membrane–water interfaces, Biophys. J. 81 (2001) 2458–2472.
[46] P.J.R. Spooner, A. Watts, Reversible unfolding of cytochrome *c* upon interaction with cardiolipin bilayers. 1. Evidence from deuterium NMR measurements, Biochemistry 30 (1991) 3871–3879.
[47] I.L. Nantes, M.R. Zucchi, O.R. Nascimento, A. Faljoni-Alario, Effect of heme iron valence state on the conformation of cytochrome *c* and its association with membrane interfaces, J. Biol. Chem. 276 (2001) 153–158.